Evaluation of wound healing effect of curcumin loaded OPL carbon nanospheres embedded Chitosan membranes

Roopesh M
Jain University
Jyothi M S
AMC Engineering College
Rajendran Velmurugan
Chulalongkorn University Faculty of Science
Gurumurthy Hegde
Christ University
Rangappa S Keri (keriphd@gmail.com)
Jain University
Khantong Soontarapa
Chulalongkorn University Faculty of Science

Research Article

Keywords: Carbon nanospheres, wound healing, MRSA infection, curcumin, chitosan

Posted Date: May 5th, 2022

DOI: https://doi.org/10.21203/rs.3.rs-1576464/v1

Abstract

Biowaste derived carbon and the biomaterial scaffolds are being used for wound healing are the focus of interest. Carbon nanospheres derived from oil palm leaves without any catalysts *via* pyrolysis were loaded with a traditional drug curcumin. The wound healing scaffolds were fabricated on the polypropylene non-woven fabric support using chitosan as the biopolymer matrix. Prepared carbon nanospheres and the scaffolds were characterized using ATR-IR and FESEM techniques. The wettability of scaffolds was examined to ensure the feasible moisture absorption ability, *in vitro* drug release profile and *in vitro* antibacterial activity against two bacterial. The *in vivo* wound healing feature of scaffolds was studied by excision wound model for MRSA infected wound. Measured % wound contraction and the bacterial count on wounds at regular time intervals proved that, the scaffold dressed with chitosan and curcumin loaded carbon nanoshperes showed an efficient reconstruction of skin through histopathological investigations.

Introduction

A restoration of damaged tissue and its integrity is referred as a wound healing process. Wound healing comprises a sequence of biochemical as well as physiological steps distributed in four phases [1, 2]. To name, firstly hemostasis driven by vasoconstriction and complementing cascades, secondly, inflammation driven by vasodilation and activation of macrophage. Third one being proliferation involve epithelialization, angiogenesis and granular tissue formation. This phase also involves a provisional deposition of a matrix. The last one is remodeling phase, where, extracellular matrix deposition takes place in well-organized network would form, formation of myofibrolasts and wound contraction are also involved in this phase [3]. The devastations at any phase of wound healing process would lead to an unhealable chronic ulcer [4]. Hence, well planned management of wound healing and its related complications has become significant in recent years in order to increase the quality of life. Infection of wound is still a dispute for wound care professionals. Several strategies have been attempted to check the wound infections. Among them practicing an applicable dressings having enough potential to inhibit the bacterial infiltration at the time of wound restoration is crucial one [5]. Methicillin-resistant *Staphylococcus aureus* (MRSA) is the most conjoint infection distressing several thousands of patients every day [6, 7]. Anchoring antimicrobial negotiators to enhance the natural bactericidal efficiency of few polymers is one of the best ways to combat the challenges associated with infected wounds [8, 9].

An advanced and ideal wound dressing should uphold the microenvironment and discourse all the limitations accompanied with nature and injury state of wound. The dressings must allow enough gaseous exchange and shelter the peri-wound skin against maceration. A balanced moisture and an efficiency to act as barriers for infections are the key requirements [10]. Overall, the dressing must promote angiogenesis with less perfusion, immune cells modulation, invasion enhancement, fibroblasts migration and keratinocytes in the healing process along with treatment or prevention of infection [11–13].

Chitosan (Ch) is enormously used dressing materials which is known to accelerate the healing process [14, 15]. Stimulating the migration of mononuclear and polymorphonuclear cells and enhancing the reepithelialization and reconstruction of regular skin are the features of Ch [16]. Additionally, excess granulation tissue and formation of scar is also avoided, when chitosan is used [17, 18]. Koyano et al. has proved the fibroblasts growth by using poly vinyl alcohol/Ch hydrogel [19]. A film forming, spongy property of Ch and its interaction with electronegative components at the cell interfaces alter the permeability and seepage of intracellular components such as protein and electrolytes [20]. Chitosan dressing optimized by polyphosphate enhanced blood clotting, platelet adhesion and aided faster thrombin generation [21]. A composite with TiO_2 and poly(N-vinylpyrrolidone) showed an excellent antimicrobial feature and better biocompatibility towards NIH3T3 and L929 fibroblasts [22].

Along with several composites, carbon based nanomaterials/Ch membranes and hydrogels have been emerging in recent years due to their acceptable biological environment [23, 24]. Single and multi-walled carbon/Ch [25], carbon dots doped with cerium [26], carbon nanotubes and fullerenes [27], nitrogen doped [28] and lanthanum doped carbon quantum dots [29] and many have been explored. Among various geometrical carbons, spherical shaped ones are proved to have less toxicity and greater biocompatibility [30]. High surface area of carbon nanospheres (CNS) owing to greater ability to conjugate with biomolecules *via* feasible bonds, its affinity and stability towards chemicals are the vital contributions of CNS for bio-related applications [31].

Our previous study has elaborated the usage of oil palm leaves derived CNS [32] and sago bark derived CNS [33] for cell imaging as well as targeted drug delivery towards cancerous cells. Another study from our group reported curcumin (Cur) loaded TiO_2/Ch scaffolds for infected wound healing process [34]. These investigations have motivated the present work, wherein, oil palm leaves derived CNS were loaded with curcumin and examined for its MRSA infected wound healing competence (*in vivo* and *in vitro*). Fabricated wound dressings were characterized in detail, wettability characteristics, *in vitro* drug release profile, *in vitro* toxicological test, antibacterial test against *Escherichia coli* and *Staphayllococcus aureus*, *in vivo* wound healing ability and the MRSA infection control studies are elaborated.

Materials And Methods

Materials

Oil palm leaves were collected from local farms in Malaysia. Chitosan was gifted by SS membranes, Thailand. Curcumin was obtained from Vidya Herbs, India. Polypropylene non-woven support was purchased from local shops of Bangkok. Chemicals such as ethanol, dimethyl sulfoxide (DMSO), phosphate buffer (PBS) were procured from Merck. An agar medium was obtained from Thermo Fischer Scientifics.

Synthesis of CNS

Collected oil palm leaves were cleaned; the midribs were separated and dried at 60 ^{o}C in oven until they are moisture free (48 hours). Restsch-ZM 200, Germany was used to mill the dried leaves and milled product was sieved with a sieving machine of 62 µm to obtain fine powder of uniform size. CNS was obtained by subjecting the bio-waste powder to pyrolysis process with an aid of Nabertherm tube furnace. With 5 ^{o}C per min heating rate, the temperature was reached to 600 ^{o}C and pyrolyzed for 2 h, under nitrogen atmosphere. Dilute HCl (1 mM) was used to wash the slurry to get rid of impurities. More details of the synthesis and the morphology of CNSs can be obtained from [32].

Loading of Cur to CNS

The 100 mg of CNS was dispersed in ethanol of 50 mL and sonicated for 20 min. Cur was added to the mixture, sonicated and stirred for 15 min for 5 h. The mixture was kept undisturbed for 24 h, filtered and dried to get curcumin loaded CNS. The obtained product will be addressed as Cur/CNS for convenience.

Wound dressings fabrication

The Ch solution was obtained by dissolving 1 g of Ch in 1% acetic acid solution (100 mL). Four dressing membranes, one with only Ch on non-woven support (S/Ch), second one with Cur (200 mg) and Ch (S/Ch/Cur), third one with Ch and CNS (S/Ch/CNS) and the last one with Ch and 200 mg of Cur loaded CNS (S/Ch/Cur/CNS) were prepared. For the preparation of dressings, the homogeneous suspensions of respective dressings were casted on the PP non-woven substrate. The membranes were dried in over at 60 ^{o}C and used further for *in vivo* and *in vitro* wound healing studies.

Characterization of wound dressings

Before moving on to characterization of wound dressing materials, once the drug loading was confirmed, Cur, obtained CNS and Cur/CNS were characterized to confirm the loading of Cur in CNS using Brucker ECO-ATR-IR spectrophotometer. The CNS/Cur embedded Ch matrixe were further characterized by UV-Visible spectrophotometer and ATR-IR spectroscopy. The surface morphology of the prepared scaffolds was analyzed by Field Emission Scanning Electron Microscope (FESEM) JSM-700 1F model. The drug release studies of were investigated by Shimadzu 1800 UV-Visible spectrophotometer.

Water adsorption studies

As the balanced moisture content is important for wound dressings, the water adsorption ability of prepared dressing materials was estimated by considering 5×2 mm of the same. The membranes were dried in oven and were immersed in water for 24 h. Membranes were then blotted with blotting paper to remove excess water. The dry weight and wet weight of the membranes were noted to calculate the water uptake ability of dressing materials. The tests were done in triplicates and the average is considered.

In vitro **cytotoxicity studies**

Formerly to zone inhibition test (antibacterial) for wound dressing scaffolds, cell viability test was performed for powdered samples (CNS and Cur-CNS) *via* MTT assay. To prepare stock solution, in a PBS

solution, 5 mg/mL of MTT was dissolved and the formed formazan crystals were filtered and stored at -20 ^{o}C. A diluted MTT solution of ratio 1:10 and L929 cells were used for experimentations. In 96-well plate, 100 µL/1000 cells were incubated for 48 h, at 37 ^{o}C and under 5% carbon dioxide environment. Cells with just the media were deliberated as control ones and for others, the powder samples were injected to each plate, and the incubation was continued for 24 h. After removing the media, 100 µL MTT was injected to each wells and subjected to incubation for 2 h. The cells were further washed, gathered in DMSO and examined at 570 nm in UV spectrophotometer.

In vitro **drug release studies**

An *in vitro* drug release profile of S/Ch/Cur and S/Ch/Cur/CNS were performed *via* direct suspension method. Three sets of experiments were performed to each membrane and the average values are considered for the evaluation. Membranes of size 2×2 cm were immersed in a 200 mL of PBS solution with 10 mM concentration. The pH of the solution was 7.4 and incubated in shaker water bath at 37 ^{o}C. The experiment was performed for 14 days and the amount of drug released was analyzed every day. To calculate the % drug released, 2 mL of sample was taken out and the study samples were replenished by the same amount. 2 mL test sample was concentrated in centrifuge, the drug is homogenized in 10 mL of ethanol and evaluated for its concentration using UV-Visible spectrophotometer at 423 nm.

In vitro **antibacterial studies**

The antibacterial test for prepared membranes was performed against one gram positive and one gram negative bacterial, *Escherichia coli* and *Staphayllococcus aureus*, respectively. In a petri plate, a disc shaped membranes of 12 mm diameter were placed on LB agar medium inoculated with 10^5 CFU/mL of cell concentration. The plates were refrigerated for 1 h for an appropriate diffusion and then incubated for 24 h at 37 ^{o}C. Inhibition zone for each membrane was measured using Vernier caliper.

In vivo **wound healing studies**

Details on animals and experimentation protocols

Spargue dawley male rats of six weeks old and of 100–120 g of body weight were considered for the *in vivo* experiments. The rats were permitted to water with full access and a traditional chow diet. An alternative dark and light cycles of 12 h each was maintained. Xylazine and ketamine were used for anesthesia and the standard surgical techniques were followed. The randomized animals were teamed into four groups (Group I = Sham control; Group II = MRSA Infection control; Group III = Infection + S/Ch/CNS; Group IV = Infection + S/Ch/Cur/CNS) each with five animals. The guidelines given by Institutional animals' ethics committee, SSCP/203/2019-20, Sree Siddaganga College of Pharmacy, Tumkuru, Karnataka, were followed for the conduction of experiments.

Creation of wound (excision wound model)

A cocktail of xylazine and ketamine of 10 mg/kg and 70 mg/kg body weight were injected to the experimental animals for which the dorsal skin was shaved. A wound of known area (2 cm^2) was made under aseptic environments on the thoracic region. The stress and pain for the experimental animals was reduced by the administration of analgesic. For wound healing, the dressings fabricated in the study were positioned in such way that, the active components of the membranes faced the wound. With an aid of crepe band, the dressings were wrapped and the rats were housed in above mentioned conditions. The restoration of skin on the day of wound excision, after one week (7th day) and two weeks (14th day), was measured by analyzing the boundaries of wound. A percent of wound contraction and the epithelization was examined by taking histograms for the last day of the study.

Presence of bacteria on the wound

On the wound contraction measurement days, day 0, 7 and 14, the wounds were swabbed with cotton, sliced and placed in a sterile physiological saline (1 mL). The mixture was vortexed and the bacterial cells were released to saline. From the suspension, 100 µL was pipetted, added to agar plate and incubated for bacterial growth (16 h, 37 ^oC). The colonies of MRSA were counted for further studies.

Measurement of wound contraction and analysis of histograms

The size of the wound was measured by tracing the wound on the transparent paper on day 0, 7 and 14. The traced wound boundaries were then shifted to graph sheet of 1 mm^2 to calculate the size of the wound. With an aid of wound size on zeroth day, the contraction in the wound was calculated by Eq. 1. For histograms, the sectioned biopsies of wound area on the last day (14th day) were fixed in formalin solution of 10%. The collected samples were implanted in paraffin wax and haemotoxylin-eosin staining was done. The samples were examined using light microscope.

$$\%Woundcontraction = \left(\frac{Initialwoundsizeonzerothday - Specificdaywoundsize}{Initialwoundsizeonzerothday} \right) \times 100$$

… 1

Histograms of the skin tissues collected at 14th day of the study were analyzed. The cross-sectional skin specimens of full-thickness were collected and examined for histopathological alterations.

Statistics

The data were taken in triplicates, wherever necessary. The results are stated in mean ± SEM. The data were analyzed using a software GraphPad Prism 5.0, San Diego, USA. The statistical assessments were done between the groups treated with drugs and control ones. Tuki annova method was applied for the same. The bacterial wound count and contraction of wound were examined by same method and multiple range test of Bonferroni's applied for *post hoc* investigations.

Results And Discussion

Material characterization

The detailed characterization of synthesized CNS was given in supplementary information, SI (Fig. 1 of SI). A spherical form with uniform size distribution with a diameter of 35–45 nm was observed for CNS and is epitomic for drug loading. The EDAX spectra showed maximum percentage of carbon, 82% and minimal amounts of oxygen and calcium. Obtained spherical shape was also verified by TEM micrographs. In the next step, the Cur loaded CNS was characterized using UV-Visible spectra and ATR-IR, the obtained results are provided in Fig. 2 and Fig. 3 of SI. The UV-visible absorbance peak for Cur alone was obtained at 435 nm and the same peak is observed for CNS loaded with Cur.

The ATR-IR spectra and FESEM micrographs of scaffolds i.e., nonwoven fabric (support), chitosan coated membrane, CNS loaded chitosan membrane and CNS/Cur loaded chitosan membrane are provided in Fig. 1 and Fig. 2, respectively. For substrate (polypropylene non-woven fabric), ATR-IR peaks at 2929, 1716 and 970 cm^{-1} were assigned to CH_3, C = O and C-O-C groups of polypropylene [35]. A peaks from 1000 to 1600 cm^{-1} attributes to the oxygen containing functionalities of chitosan [36] for S/Ch sample. The peaks at 1066 and 1028 cm^{-1} are attributed to C-O stretching vibrations. A peak at 1153 cm^{-1} was due to the C-O-C bridge asymmetric bending of chitosan [37]. For S/Ch/Cur, the overlapped stretching frequencies for alkene C = C and C = O is observed at 1628 cm^{-1}. A peaks in the range of 3200 to 3500 $cm^{-1}$are attributed to O-H groups, atomatic stretching of C = C is at 1427 cm^{-1}. A high intensity band at 1512 cm^{-1} is for the mixed vibrations including υ (C = O) in-plane bending vibration around aliphatic δ CC-C, =O, δ CC-H in-plane bending vibrations of aromatic carbon of keto and enol configurations and υ CC bonds of the same of curcumin [38]. A peaks at 1100 and 1560 cm^{-1} of S/Ch/CNS are attributed to N-H bending of primary amines and C-N stretching of aliphatic amine. Peaks for C-OH for the cellulose derived carbon framework were observed at 3400 to 3600 cm^{-1}. For the final wound dressing material which is composed of peaks from non-woven polypropylene substrate, chitosan, curcumin and CNS were overlapped and very slight shifts were observed.

FESEM micrographs of all prepared scaffolds are provided in Fig. 3. The fiber nature of nan-woven fabric was evident from Fig. 3(a). The coating of chitosan, S/Ch and curcumin, S/Ch/Cur (Fig. 3(b) and 3(c)) masked the fiber nature of substrate material, indicating the coating of them on the polyprolylene fabric. The micrographs of S/Ch/CNS and S/Ch/Cur/CNS showed the aggregated lumps on the fabric surface. The inset zoom in pictures provided for both the samples highlight the incorporation of CNS (nanospheres). It is also noted that, the nanosphere nature of CNS remained same even after loading of Cur.

Wettability test for wound dressings

Water flux is an important parameter for wound dressing materials, the material must be able to absorb water and maintain the feasible moisture conditions. Though the required moisture content for the same is unknown, water wettability of the prepared dressings is measured and the results with respect to water adsorption of dressings with CNS, Cur/CNS and Cur are compared. Calculated water wettability in percent

is demonstrated in Fig. 3. The dressing Ch showed the water uptake of 255.24 ± 10.66%, it increased to 384.19 ± 14.70% for the one with CNS. Water uptake was about 362.78 ± 18.83% for S/Ch/Cur material and 475.37 ± 8.98% for the dressing which contained CNS loaded with Cur. Chitosan is hydrophilic in nature and was able to absorb enough amount of water. With the addition of CNS, which are porous in nature, the water uptake increased. The porous nature of carbon nanospheres and the functionalities of curcumin synergistically contributed to water adsorption and hence wound dressing S/Ch/CNS/Cur showed 475.37 ± 8.98%. The water adsorption proved that, S/Ch/CNS/Cur material possessed a great ability to adsorb enough moisture and support wound healing process by adsorbing the moisture content produced during the progression of wound.

MTT assay

Dose dependent cell viability is a significant factor for the wound healing applications. Such responses for considered L929 cell lines on treating with Cur and Cur/CNS were investigated and the percent cell viability is given in Fig. 4. From ancient times, curcumin has proven its efficacy in wound healing, though the cell viability was neglected. However, recent research is considering cell proliferation assay as crucial component [39, 40]. In present study, the percent cell viability for the Cur treated cells was of 99.82 ± 0.32% at lower concentrations (25 µg/mL) and it reached to 95.29 ± 0.73% for 200 µg/ml. For Cur/CNS, the values were 99.25 ± 0.56% and 93.03 ± 0.24% at lower and higher concentrations, respectively. The obtained values clearly confer the feasibility of Cur loaded CNS for the wound healing applications.

In vitro **drug release studies**

In vitro drug release is crucial as far as nanoparticles are considered, due to its dependency on many features such as 1) diffusion of the drug through the nanomaterials, 2) diffusion *via* hydrated pores within the nano materials, and 3) due to the cleavage of bonds in case of degradable ones. In present work, case one and two are expected. The results of *in vitro* drug release studies are provided in Fig. 5. The water uptake studies have clearly demonstrated the maximum water affinity of the final wound dressing scaffold i.e., S/Ch/Cur/CNS, which would lead to the diffusion of Cur through water filled pores of CNS. Over the time, the drug entrapped in the polymer matrix is released due to the bulk polymer degradation. But, with S/Ch/Cur, the release of drug is directly from the polymer matrix, allowing the faster diffusion and hence greater drug release of nearly 62.3% on the day one itself. Almost all the drug is released within 5 days and it attained the saturation level. For S/Ch/Cur/CNS, first day drug release was minimal and is about 35.2%, the gradual release is observed for the next 9 days owing to the existence of CNS.

In vitro **antibacterial activity**

In vitro antibacterial activity was performed for the membrane samples, including bare nonwoven fabric and chitosan membrane. The zone of inhibition test was carried out and the pictures are provided in Fig. 6. For both gram + ve (Fig. 6 (a)) and gram –ve (Fig. 6 (b)) bacteria, the zone of inhibition for nonwoven fabric (M0) was negligible. For membrane loaded with Cur (M1), the values were 6.1 ± 0.2 and

10.2 ± 0.1 mm, for membranes with Ch alone (M2), 7.21 ± 0.1 and 6.9 ± 0.4 mm, for membranes with S/Ch/CNS (M3), 8.3 ± 0.9 and 11 ± 0.8 mm and for S/Cur/CNS loaded membranes (M4), 8 ± 0.6 and 11 ± 1.0 mm, for gram + ve and gram –ve bacteria, respectively. Curcumin being natural polyphenolic flavonoid offers several biological applications. For antibacterial agents, the bacterial cytokinesis assessed by the stability and congress of FtsZ protofilaments is a key component [41]. The inhibition of congress dynamics of the FtsZ in Z-ring by curcumin is uttered to suppress the cell proliferation [42]. The interaction of carbon with bacterial membrane is found to destroy the cell membrane resulting in antimicrobial nature [43, 44]. In present work, a feasible antimicrobial feature is confirmed for all four membranes S/Ch, S/Ch/Cur, S/Ch/CNS and S/Ch/Cur/CNS, except nonwoven fabric, conferring the further use of these membranes for *in vivo* applications.

In vivo **wound healing studies**

In vivo wound healing studies were performed for four groups, sham control, infection control, S/Ch/CNS and S/Ch/Cur/CNS. The studies were not conducted for S/Ch and S/Ch/Cur as they were detailed in our previous studies [34]. The representative camera pictures of assessment of wound healing characteristics for the membranes are presented in Fig. 7 for day 0, 3, 7, 10 and 14. The respective calculated % wound contraction is provided in Fig. 8. For sham and infection control at day 3, the wound contraction was just 4 and 3.85% whereas, for S/Ch/CNS and S/Ch/Cur/CNS, it was 10.65 and 14%. For day 7, sham control and S/Ch/CNS showed nearly same % wound contraction. However, infection control showed 28.4% and S/Ch/Cur/CNS showed 39.5% of wound contraction. At day 10, S/Ch/Cur/CNS gave a highest wound contraction and was of 76% and the control groups showed ~ 45%. At day 14, the wound contraction was maximum and almost healed. Control groups still possessed ~ 25% of wound, S/Ch/CNS groups showed ~ 11% wound and our material of interest S/Ch/Cur/CNS possessed 4.5% of wound.

Wound closure was lesser for sham and infection controls and was greater for the one with Cur and CNS. In early wound healing days (3rd day), the wound closure was almost similar. Cur is known to reduce the inflammation and induce cell proliferation leading to the damage tissue reconstruction. Cur is proven to typically act as an antioxidant since free radicals are deliberated to be the major reasons for inflammation thru wound healing course [45]. The contribution of Cur in every step of wound closure mechanism is elaborated by many researchers. In the first step itself, Cur suppress the inflammation by scavenging the reactive oxygen species. Gopinath *et al.*, have shown the in vitro antioxidant ability of Cur which was dispersed in collagen matrix via lipid peroxidation process [46]. Gadekar *et al.*, in the *in vivo* study, demonstrated the suppression of keratinocytes and fibroblasts damage induced by H_2O_2 [47]. In fibroblasts proliferation step, curcumin at its optimal dosage enhances the infiltration of fibroblasts [48]. The next step is of granulation of tissues, where a protein marker hydroxyproline is measured which confers the collagen synthesis. Gopinath and group also worked on this process and showed the involvement of Cur in the granulation of tissues which further increases the re-epithelialization and provides the basal backing for the migration of epithelial cells which would further help the wound closure [46]. As the wound healing process progress, apoptosis plays a crucial step in eliminating the undesirable inflammatory cells. Though, the exact mechanism is unclear, the functioning of Cur in this

step is demonstrated [48]. The biocompatibility of the CNS was elaborated by one of our co-author, wherein CNS was loaded with a florescent dye and was used for cell imaging and drug delivery purpose [32]. The proven antibacterial effect of CNS and the chitosan have facilitated the synergistic effect and accelerate the wound healing process.

Histopathological investigations

To understand the reconstruction of skin structure, histograms play a key role. Histograms of skin tissues from considered four groups at day 14, are provided in Fig. 9. Histology of Group I skin showed normal histo-architecture with normal epithelization (Fig. 9(a)) and infection control, Group II skin showed partial reepithelization as highlighted with an arrow in Fig. 9(b) and focal epidermal hyperplasia. Group III skin tissue showed granulation with neo angiogenesis as highlighted with an arrow in Fig. 9(c) and diffused epidermal hyperplasia. Group IV, treated with S/Ch/Cur/CNS wound dressing showed a normal histology which is in accordance with Group I histogram. The histograms confirm that, the reconstruction of skin tissue was with norma architecture for Group IV, proving the potency of considered dressing as the best wound healing material.

Conclusions

A successful fabrication of Ch based Cur loaded CNS on PP non-woven support was confirmed. The spherical nature of CNS remained same even after loading of Cur which is evident from FESEM images. Embedded drug in the CNS framework resulted in feasible drug release pattern. Porous CNS and rich functionalities of Cur together contributed to the feasible water adsorption by the scaffolds and the wound dressing S/Ch/CNS/Cur showed a maximum wettability of 475.37 ± 8.98%. Nearly 93 to 99% cell viability was observed from MTT assay proving the non-toxic nature of prepared scaffolds. The inhibition of cell proliferation by Cur and the destruction of cell membrane by carbon material resulted in good antimicrobial activity for Cur loaded CNS. Nearly 96.5% wound contraction was observed for our material of interest on the 14th day of study and the regain of skin structure was confirmed by histogram showing normal reepithelization and granulation.

Declarations

Acknowledgments

We are grateful to the Jain University, Bangalore for providing partial facility. Authors would like to acknowledge S S Membranes Co., Ltd., Bangkok, Thailand for providing required membrane material.

Funding

The authors declare that no funds, grants, or other support were received during the preparation of this manuscript.

Competing Interests

The authors have no relevant financial or non-financial interests to disclose

Author Contributions

All authors contributed to the study conception and design. Material preparation, data collection and analysis were performed by Roopesh M, Jyothi M S, Rajendran Velmurugan, Gurumurthy Hegde, Rangappa S. Keri, Khantong Soontarapa. The first draft of the manuscript was written by Roopesh M and Jyothi M S and all authors commented on previous versions of the manuscript. All authors read and approved the final manuscript

References

1. Tarrahi R et al (2022) The latest achievements in plant cellulose-based biomaterials for tissue engineering focusing on skin repair. Chemosphere 288:132529
2. Xia C et al (2021) *A Feasible Strategy of Fabricating of Gold-Encapsulated Dextran/Polyvinyl Alcohol Nanoparticles for the Treatment and Care of Wound Healing*.Journal of Cluster Science, : p.1–9
3. Bielefeld KA, Amini-Nik S, Alman BA (2013) Cutaneous wound healing: recruiting developmental pathways for regeneration. Cell Mol Life Sci 70(12):2059–2081
4. Pannerselvam B et al (2021) In vitro Cytotoxicity and Antibacterial Activity of Optimized Silver Nanoparticles Against Wound Infectious Bacteria and Their Morphological Studies. J Cluster Sci 32(1):63–76
5. Yu J et al (2022) Injectable Methylcellulose and Hyaluronic Acid Hydrogel Containing Silver Nanoparticles for Their Effective Anti-microbial and Wound Healing Activity After Fracture Surgery. J Polym Environ 30(4):1330–1343
6. Dantes R et al (2013) National burden of invasive methicillin-resistant Staphylococcus aureus infections, United States, 2011. JAMA Intern Med 173(21):1970–1978
7. Hassan A et al (2018) Development of Anti-bacterial PVA/Starch Based Hydrogel Membrane for Wound Dressing. J Polym Environ 26(1):235–243
8. Gholami H et al (2018) Vegetable Oil Based Polyurethane Containing 1,2,3-Triazolium Functional Groups as Antimicrobial Wound Dressing. J Polym Environ 26(2):462–473
9. Altaf F et al (2021) Synthesis and Characterization of PVA/Starch Hydrogel Membranes Incorporating Essential Oils Aimed to be Used in Wound Dressing Applications. J Polym Environ 29(1):156–174
10. Rezvani Ghomi E et al (2019) Wound dressings: Current advances and future directions. J Appl Polym Sci 136(27):47738
11. Mosaad KE, Shoueir KR, Dewidar MM (2021) Fabrication of Multifunctional Wound Dressing Composite Biomaterials Composed of Ag/Mg-Hydroxyapatite Doped Electrospun Poly (Vinyl Alcohol) Nanofibers for Skin Tissue Regeneration. Journal of Cluster Science

12. Rafati Z et al (2020) Honey-Loaded Egg White/Poly(vinyl alcohol)/Clay Bionanocomposite Hydrogel Wound Dressings: In Vitro and In Vivo Evaluations. J Polym Environ 28(1):32–46
13. Mohebian Z et al (2022) A Novel Aloe Vera-Loaded Ethylcellulose/Hydroxypropyl Methylcellulose Nanofibrous Mat Designed for Wound Healing Application. J Polym Environ 30(3):867–877
14. Hajji S et al (2022) Development of Nanocomposite Films Based on Chitosan and Gelatin Loaded with Chitosan-Tripolyphosphate Nanoparticles: Antioxidant Potentials and Applications in Wound Healing. J Polym Environ 30(3):833–854
15. Shahzadi L et al (2018) Biocompatibility Through Cell Attachment and Cell Proliferation Studies of Nylon 6/Chitosan/Ha Electrospun Mats. J Polym Environ 26(5):2030–2038
16. Kojima K et al (1998) Collagen typing of granulation tissue induced by chitin and chitosan. Carbohydr Polym 37(2):109–113
17. Pal P et al (2021) Applications of chitosan in environmental remediation: A review. Chemosphere 266:128934
18. Xu H et al (2020) A Novel Approach of Curcumin Loaded Chitosan/Dextran Nanocomposite for the Management of Complicated Abdominal Wound Dehiscence. J Cluster Sci 31(4):823–830
19. Koyano T et al (1998) *Attachment and growth of cultured fibroblast cells on PVA/chitosan-blended hydrogels.* Journal of Biomedical Materials Research: An Official Journal of The Society for Biomaterials, The Japanese Society for Biomaterials, and the Australian Society for Biomaterials, **39**(3): p.486–490
20. Muzzarelli R et al (1990) Antimicrobial properties of N-carboxybutyl chitosan. Antimicrob Agents Chemother 34(10):2019–2023
21. Ong S-Y et al (2008) Development of a chitosan-based wound dressing with improved hemostatic and antimicrobial properties. Biomaterials 29(32):4323–4332
22. Archana D et al (2013) In vivo evaluation of chitosan–PVP–titanium dioxide nanocomposite as wound dressing material. Carbohydr Polym 95(1):530–539
23. El-Sayyad GS et al (2020) Facile Biosynthesis of Tellurium Dioxide Nanoparticles by Streptomyces cyaneus Melanin Pigment and Gamma Radiation for Repressing Some Aspergillus Pathogens and Bacterial Wound Cultures. J Cluster Sci 31(1):147–159
24. Shaheen TI et al (2021) Benign Production of AgNPs/Bacterial Nanocellulose for Wound Healing Dress: Antioxidant, Cytotoxicity and In Vitro Studies. Journal of Cluster Science
25. Kittana N et al (2018) Enhancement of wound healing by single-wall/multi-wall carbon nanotubes complexed with chitosan. Int J Nanomed 13:7195
26. Zhang M et al (2021) Multifunctional cerium doped carbon dots nanoplatform and its applications for wound healing. Chem Eng J 423:130301
27. Murugesan S et al (2007) Carbon inhibits vascular endothelial growth factor- and fibroblast growth factor-promoted angiogenesis. FEBS Lett 581(6):1157–1160

28. Zhao C et al (2019) Nitrogen-doped carbon quantum dots as an antimicrobial agent against Staphylococcus for the treatment of infected wounds. Colloids Surf B 179:17–27
29. Wang M et al (2021) Antibacterial Fluorescent Nano-Sized lanthanum-doped carbon quantum dot embedded polyvinyl alcohol for Accelerated Wound Healing. Journal of Colloid and Interface Science
30. Wang J et al (2014) Therapeutic applications of low-toxicity spherical nanocarbon materials. NPG Asia Materials 6(2):e84–e84
31. Kumar A et al (2014) Catalyst free silica templated porous carbon nanoparticles from bio-waste materials. Chem Commun 50(84):12702–12705
32. Yallappa S, Manaf SAA, Hegde G (2018) Synthesis of a biocompatible nanoporous carbon and its conjugation with florescent dye for cellular imaging and targeted drug delivery to cancer cells. New Carbon Mater 33(2):162–172
33. Aruni A, Manaf S et al (2017) Functionalized carbon nano-scale drug delivery systems from biowaste sago bark for cancer cell imaging. Curr Drug Deliv 14(8):1071–1077
34. Marulasiddeshwara R et al (2020) Nonwoven fabric supported, chitosan membrane anchored with curcumin/TiO2 complex: Scaffolds for MRSA infected wound skin reconstruction. Int J Biol Macromol 144:85–93
35. Tang R et al (2015) *Dielectric relaxation, resonance and scaling behaviors in Sr 3 Co 2 Fe 24 O 41 hexaferrite.* Scientific reports, **5**(1): p. 1–11
36. Jyothi M et al (2019) Magnetic nanoparticles impregnated, cross-linked, porous chitosan microspheres for efficient adsorption of methylene blue from pharmaceutical waste water. J Polym Environ 27(11):2408–2418
37. Fernandes Queiroz M et al (2015) Does the use of chitosan contribute to oxalate kidney stone formation? Mar Drugs 13(1):141–158
38. Ismail E et al (2014) Synthesis and Characterization of some Ternary Metal Complexes of Curcumin with 1, 10-phenanthroline and their Anticancer Applications. J Sci Res 6(3):509–519
39. Khosropanah MH et al (2016) Analysis of the Antiproliferative Effects of Curcumin and Nanocurcumin in MDA-MB231 as a Breast Cancer Cell Line. Iran J Pharm research: IJPR 15(1):231–239
40. Khazaei Koohpar Z et al (2015) Anticancer Activity of Curcumin on Human Breast Adenocarcinoma: Role of Mcl-1 Gene. Iran J cancer Prev 8(3):e2331–e2331
41. Mun S-H et al (2013) Synergistic antibacterial effect of curcumin against methicillin-resistant Staphylococcus aureus. Phytomedicine 20(8):714–718
42. Zorofchian Moghadamtousi S et al (2014) A Review on Antibacterial, Antiviral, and Antifungal Activity of Curcumin. Biomed Res Int 2014:186864
43. Roy P et al (2021) Mesoporous carbon nanospheres derived from agro-waste as novel antimicrobial agents against gram-negative bacteria. Environ Sci Pollut Res 28(11):13552–13561
44. Jiang Y-W et al (2017) Antimicrobial carbon nanospheres. Nanoscale 9(41):15786–15795

45. Mohanty C, Das M, Sahoo SK (2012) Sustained wound healing activity of curcumin loaded oleic acid based polymeric bandage in a rat model. Mol Pharm 9(10):2801–2811
46. Gopinath D et al (2004) Dermal wound healing processes with curcumin incorporated collagen films. Biomaterials 25(10):1911–1917
47. Gadekar R et al (2012) Study of formulation, characterisation and wound healing potential of transdermal patches of curcumin. Asian J Pharm Clin Res 5(4):225–230
48. Scharstuhl A et al (2009) Curcumin-induced fibroblast apoptosis and in vitro wound contraction are regulated by antioxidants and heme oxygenase: implications for scar formation. J Cell Mol Med 13(4):712–725

Figures

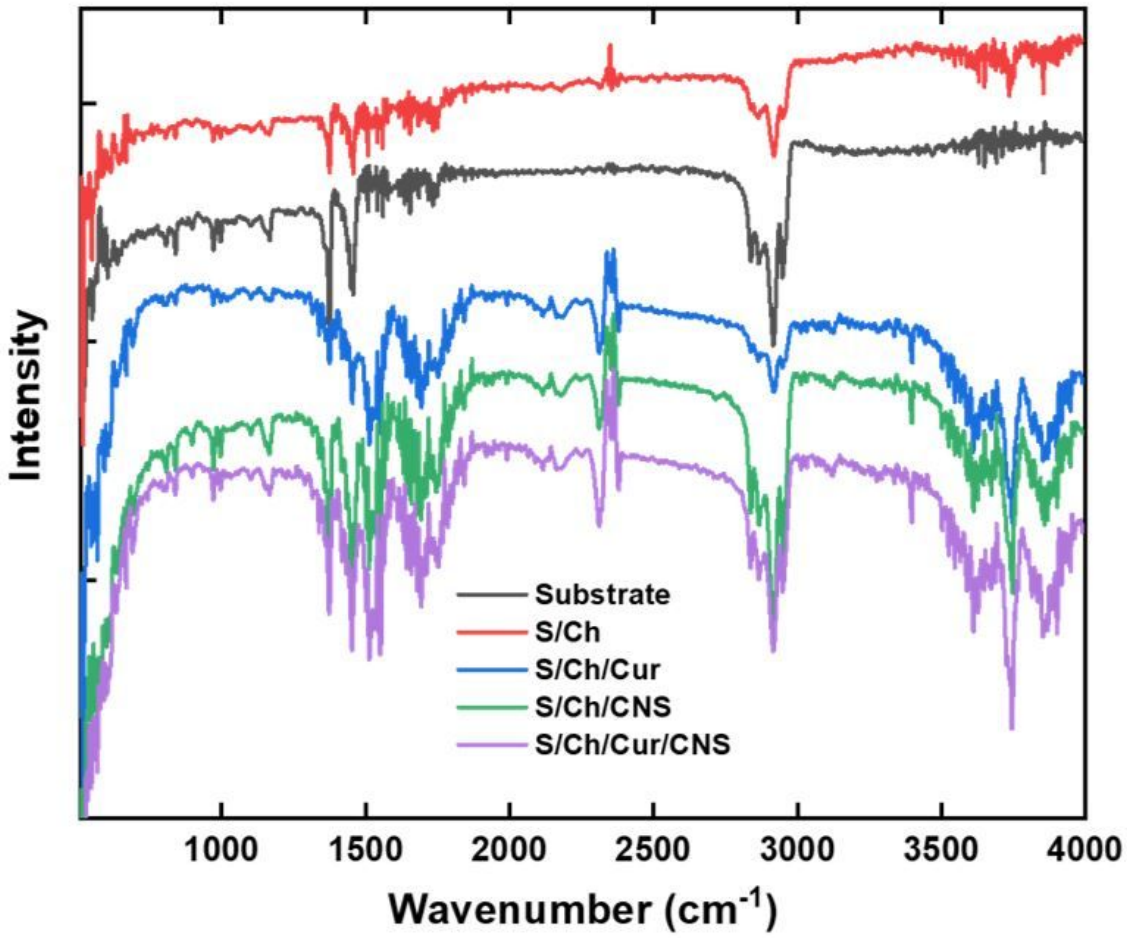

Figure 1

ATR-IR spectra of prepared scaffolds

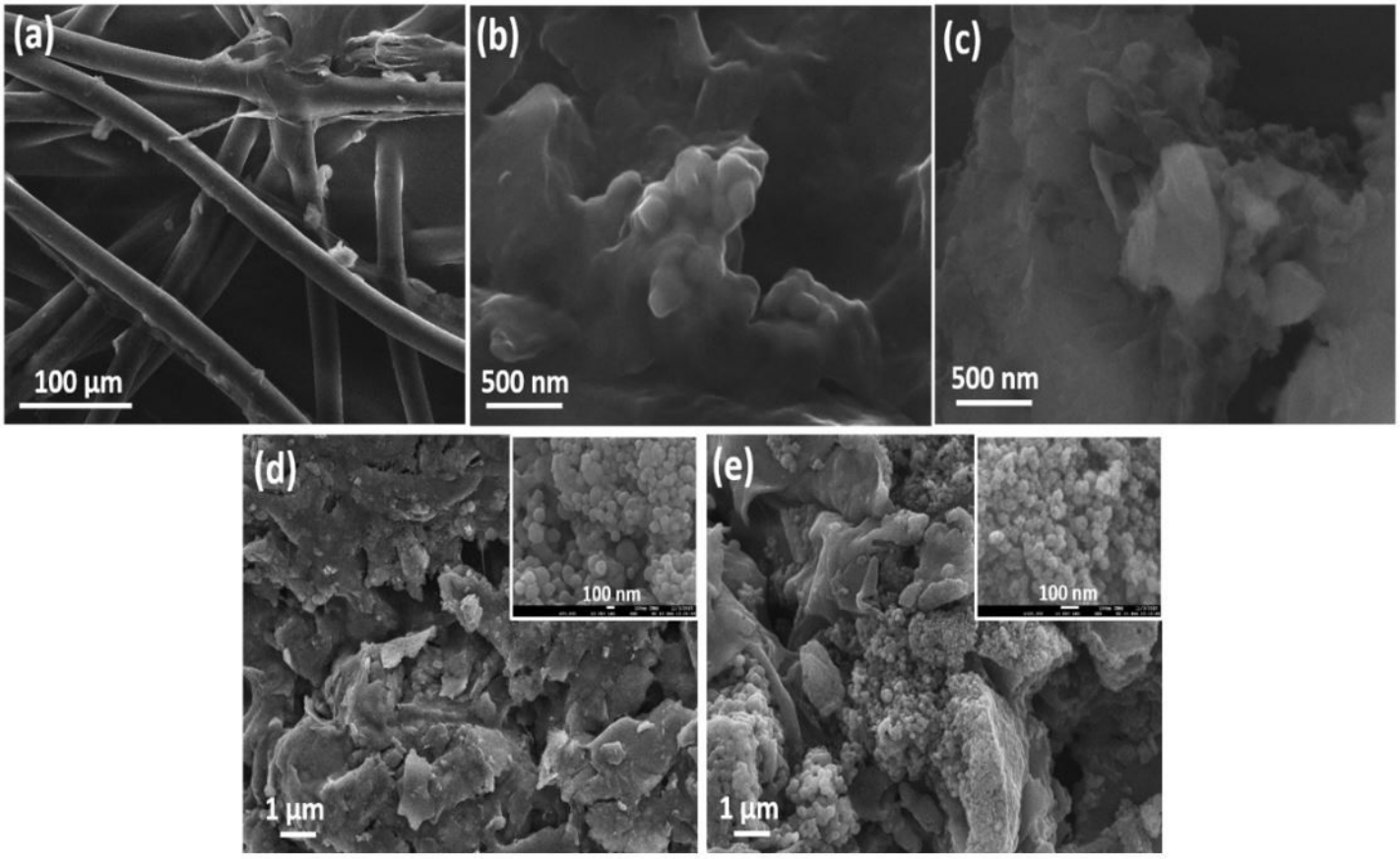

Figure 2

FESEM micrographs of a) Substrate, b) S/Ch, c) S/Ch/Cur, d) S/Ch/CNS and e) S/Ch/Cur/CNS

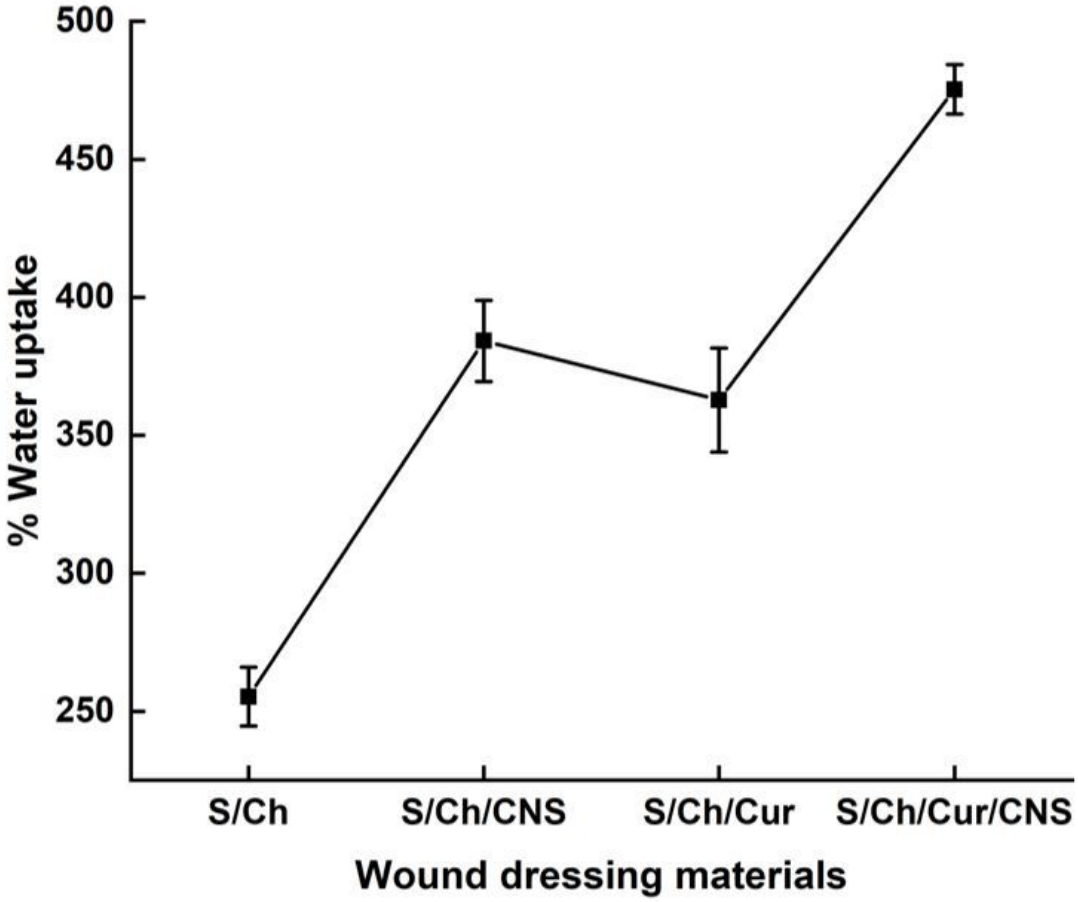

Figure 3

Water uptake capacity of fabricated wound dressings

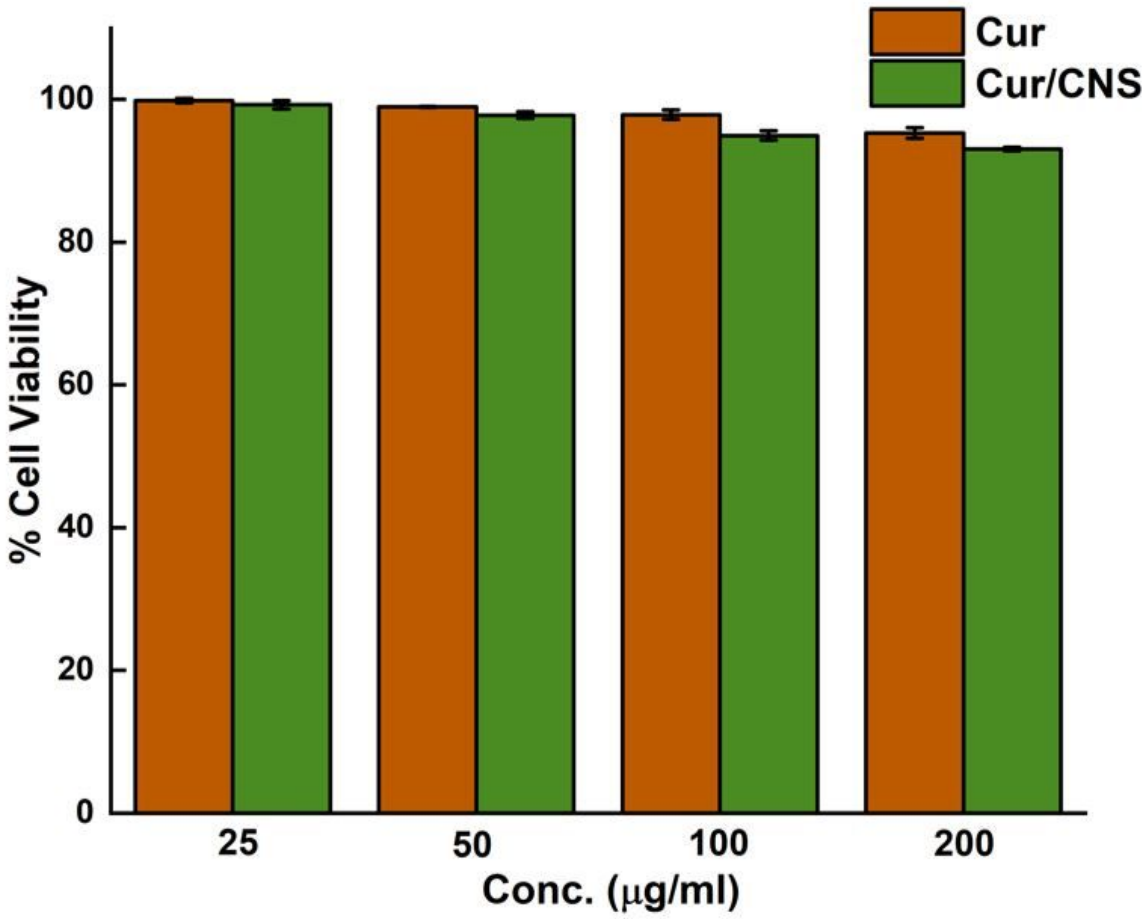

Figure 4

Percentage (%) Cell viability of Cur and Cur/CNS *via* MTT assay

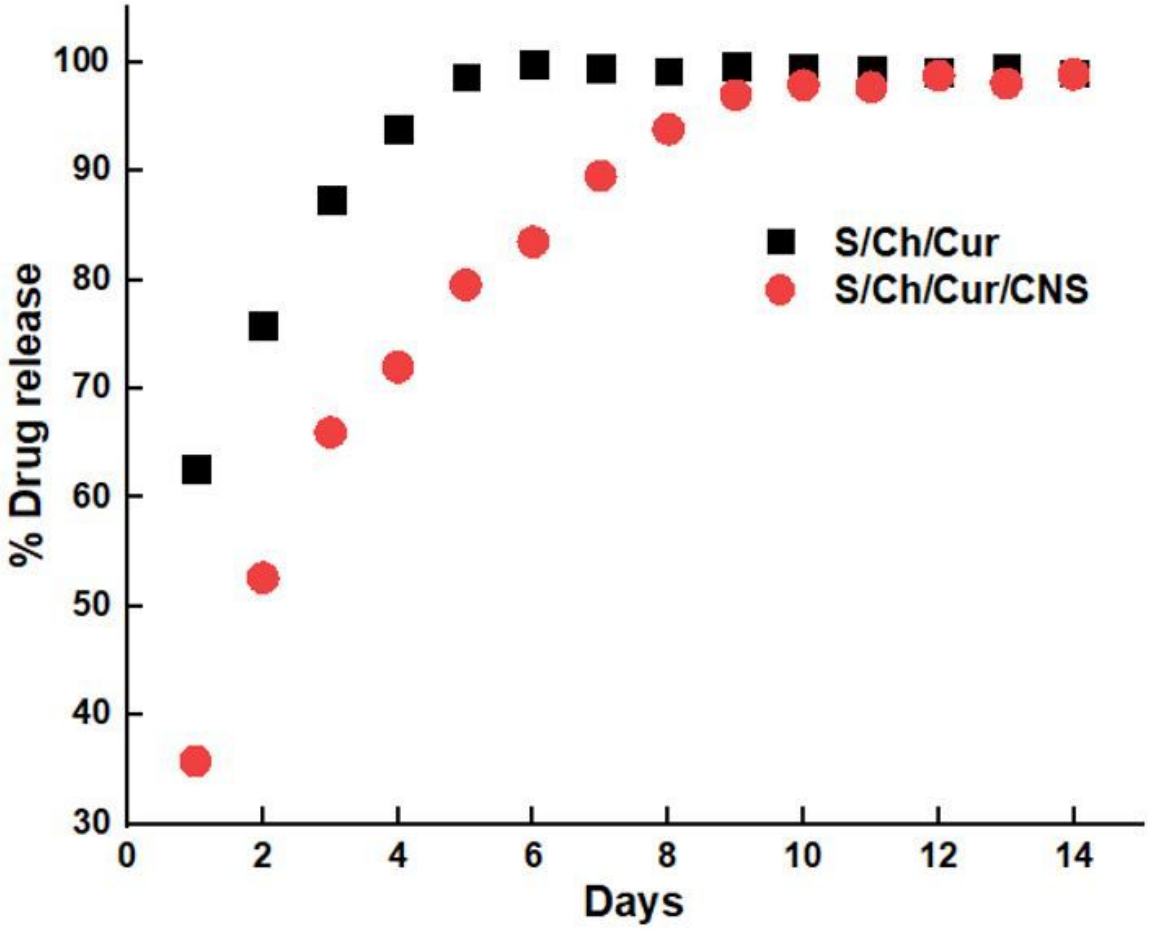

Figure 5

In vitro drug release studies for S/Ch/Cur and S/Ch/Cur/CNS

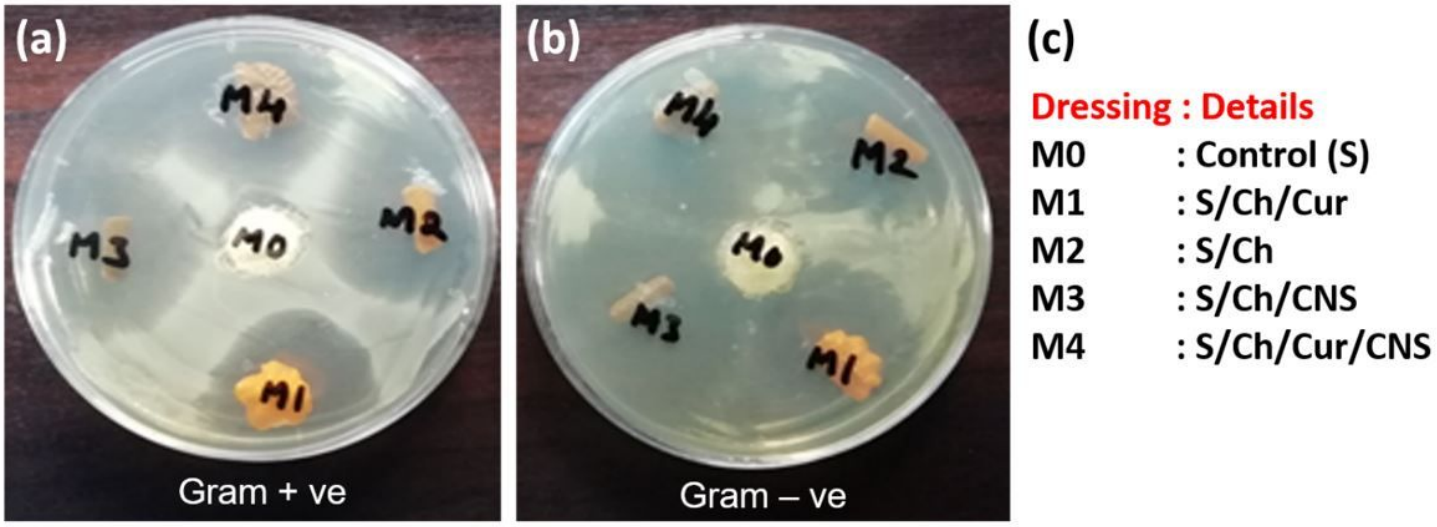

Figure 6

Camera pictures of Zone of Inhibition study for all prepared membranes

Figure 7

Photographic pictures of wound contraction for considered groups at 0, 3, 7, 10 and 14 days

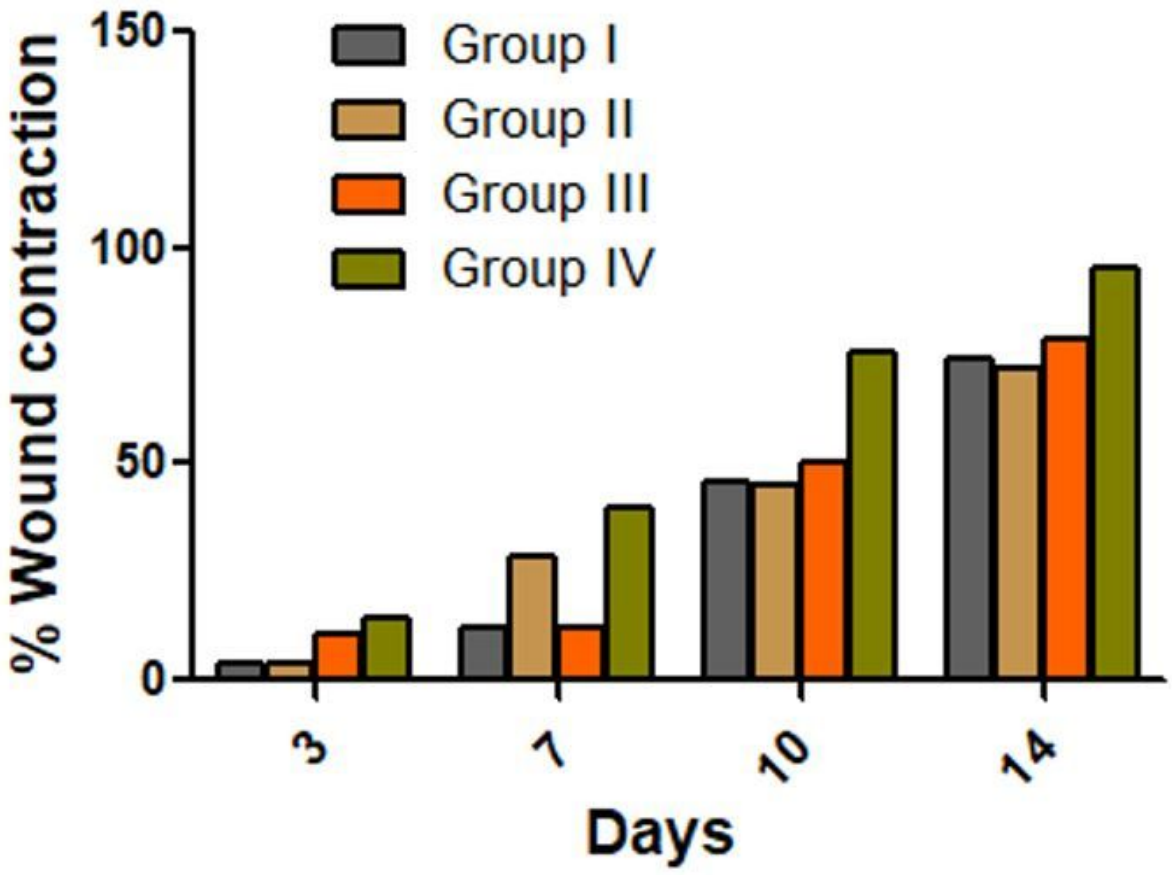

Figure 8

Percentage (%) wound contraction for Group I, II, III and IV at 3, 7, 10 and 14 days

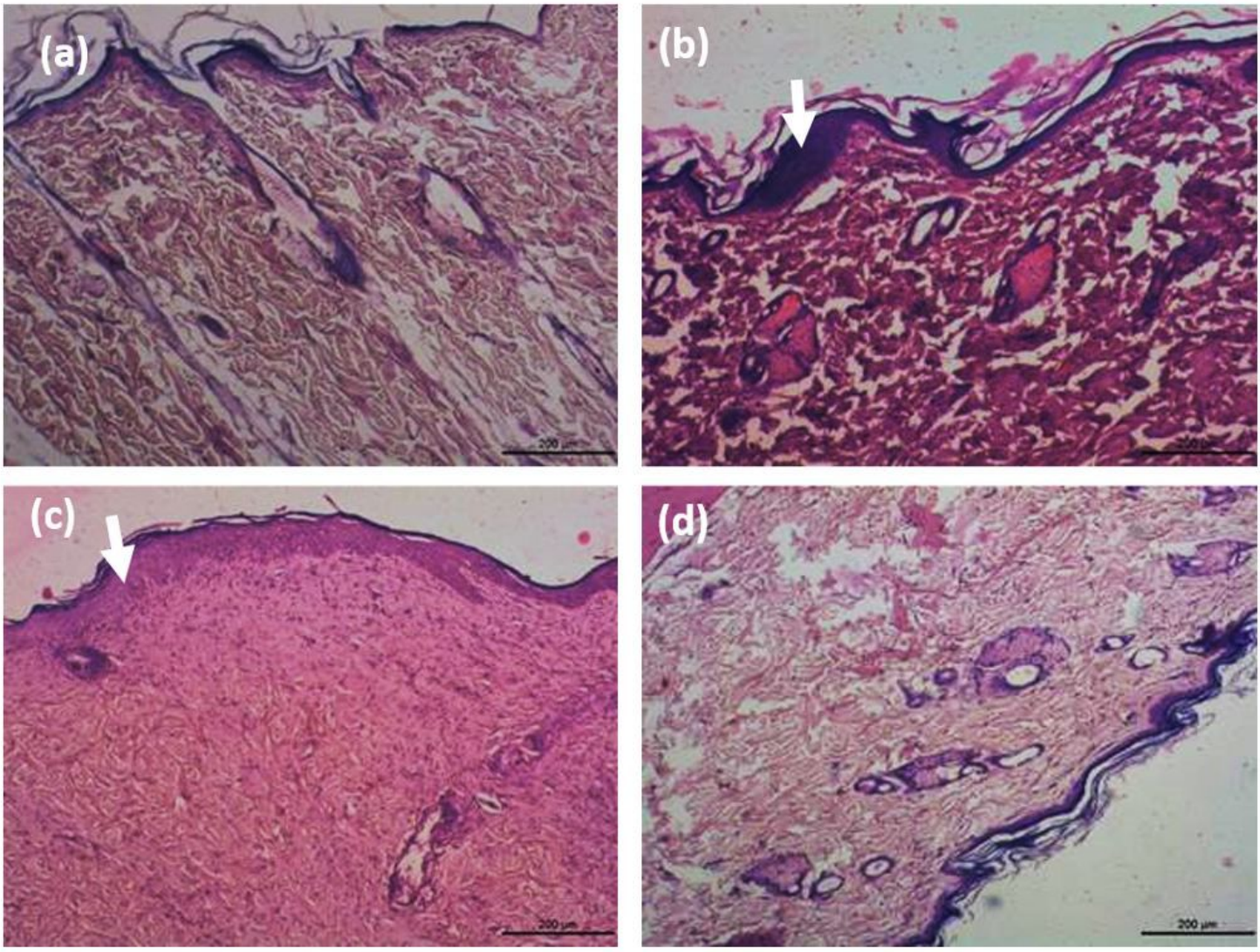

Figure 9

Histograms of skin tissue for (a) Group I; (b) Group II; (c) Group III and (d) Group IV taken at 14th day of the study

Supplementary Files

This is a list of supplementary files associated with this preprint. Click to download.

- Graphicalabstract.jpg
- SI1.docx